ISTITUTO NAZIONALE FISICA NUCLEARE

INFN/BE - 70/3
27 Maggio 1970

F. Demanins and G. Nardelli:

GAMMA RAYS FROM NEUTRON INELASTIC SCATTERING IN Fe^{56}

GAMMA RAYS FROM NEUTRON INELASTIC SCATTERING IN Fe^{56}(*)

F. Demanins

Istituto di Fisica, Università di Trieste - Italia
Comitato Nazionale per l'Energia Nucleare

G. Nardelli

Istituto di Fisica, Università di Padova - Italia

(*) Work performed at the "Laboratori Nazionali di Legnaro" (LNL INFN).

ABSTRACT

The cross sections of the $Fe^{56}(n;n'\gamma)Fe^{56}$ reaction have been measured in the neutron energy range from 1.0 MeV to 4.0 MeV. The excitation curves and the angular distributions obtained are compared with the results of an optical model calculation based on the Satchler-Sheldon formalism. The transmission coefficients used in the calculations are those derived from the optical model potentials of Bjorklund-Fernbach and Perey-Buck. The calculated cross sections based on the Moldauer theory are also compared with the experimental excitation functions. Spin and parity assignments deduced from the comparison between experimental and theoretical angular distributions are given.

1. - INTRODUCTION

By studying angular distributions of gamma-rays produced in the inelastic scattering of neutrons with nuclei, information can be obtained concerning the nuclear level scheme. The comparison of the experimental excitation functions and angular distributions with the theoretical predictions of the Hauser-Feshbach and Satchler-Sheldon formalisms, provides valuable information regarding the spins and parities of the excited nuclear levels. Particularly, the shapes of theoretical gamma-rays angular distributions are dependent upon the spin, parity and branching ratios of the nuclear levels involved.

The comparison of theoretical and experimental data may give unambigous spin assignments for the excited nuclear levels.

Several inelastic scattering experiment on Iron have been reported in the literature. Data from $Fe^{56}(n;n')$ reaction have been reported in the paper of Gilboy and Towle ([1]) and this work can be considered as example of experimental method and comparison with theoretical calculations, in these kind of measurements. By proton inelastic scattering measurements ([2,3,4,5,6,7,8]) has been obtained an extensive knowledge of the position of energy levels in Fe^{56}. Information on the spin of excited states has been obtained through measurements of the angular distributions and linear polarization of gamma-rays from oriented Co^{56} nuclei by Diddens ([9]). A study through gamma-gamma and beta-gamma coincidence measurements of the decay of Co^{56} and Mn^{56}, of gamma-rays in Fe^{56} has been performed by Kienle and Segel ([10]). As source of informations on the spins and parities as well on the position of energy levels, the time-of-flight coincidence technique has been used in the $Fe^{56}(n;n'\gamma)$ reaction by Benjamin ([11]) and recently by Armitage([12]). In this experiment a Ge(Li) spectrometer has been employed.

In the present work, the experimental results on the angular distributions and cross sections of the gamma-rays produced in the neutron inelastic scattering have been compared with theoretical calculations based on the Satchler-Sheldon ([13,14,15,16]) and Hauser-Feshbach ([17]) formalisms, over a wide range of energies. This comparison, where possible, has been employed to establish spin and parity assignments for those levels in Fe^{56} whose spin and parity were unknown or uncertain.

The present results on the excitation functions are compared with the calculated values based on the statistical theory of Hauser-Feshbach. Corrections to the formalism of Hauser-Feshbach have been proposed by Moldauer ([18,19,20]). The corrections, which take into account the level width fluctuation effect and the modification of the transmission coefficients, affect appreciably the calculated value of the inelastic scattering cross section.

In this report, the excitation functions based on the Moldauer theory are also calculated and compared with the experimental results.

2. - EXPERIMENTAL METHOD

The measurements have been performed with a pulsed beam time-of-flight technique.

The 5.5 MeV L.N.L. Van de Graaf accelerator was terminal pulsed at a repetition rate of 1 MHz with a pulse width of 5 ns. Pulses from the gamma-ray detector, NaI(Tℓ) 3"×3", located 70 cm from the sample, were timed respect to the beam reference pulses with the aid of a time-to-pulse height converter. In this manner the time distribution of the radiation arriving at the detector was measured and the gamma radiation selected from the background caused by neutrons scattered by the sample.

Two reactions were used to provide neutrons of the desired energies. The data from 1.0 MeV to 3.5 MeV were taken with a solid tritium (tritium absorbed on titanium) target using the $T(p;n)He^3$ reaction. The 4.0 MeV neutrons were obtained with the $D(d;n)He^3$ reaction, using a solid deuterium absorbed in titanium target. These targets gave neutron energy spreads from ±40 to ±35 keV and ±100 keV respectively.

The natural Iron scatterer was in the form of solid cylinder 2,5 cm in diameter and 5,0 cm long. The scattering sample was positioned at 0° with respect to the incident charged particle beam direction. The distance between the target and the center of the scattering sample was of 10 cm.

During the course of the measurements were used a long counter monitor set at 30° and a neutron NE 451 scintillation counter monitor at 90° with respect to the charged particle beam direction. The charge col-

lected at the target was also integrated simultaneously. All the data runs were made for a costant integrated charge.

The errors in the experimental data are mainly the errors propagated through the statistical deviations in the "scatterer in" and "scatterer out" counts, the subtraction of the Compton distribution from the gamma-ray photopeaks in the spectra and the statistical error in the long counter and in the scintillation monitors used for the normalization of the data runs. The errors quoted on the absolute differential cross sections also include the errors in the determination of the long counter efficiency, the efficiency of the gamma-rays detector, the self absorption of gamma-rays due to dimensions of the scatterer and the error caused by the Compton distribution due to the scattering in the sample.

Relative errors in these measurements range from 1% to 10%, while the upper limit on the errors in the determination of the cross sections has been estimated to be 20%.

3. - ANGULAR DISTRIBUTIONS AND EXCITATION FUNCTIONS FOR THE GAMMA RADIATION

We consider two typical cases of gamma-rays theoretical angular distributions, derived for a simple transition between two levels ($(n;n'\gamma)$ case) and for a two branches cascade linking three levels ($(n;n'\gamma-\gamma)$ case).

One objective of these investigations was to compare the gamma-rays angular distributions obtained in the $(n;n'\gamma)$ or in the $(n;n'\gamma-\gamma)$ processes with the Satchler-Sheldon model previsions. This comparison can yield information regarding the nuclear level spins and multipole mixing ratios of the gamma-ray transitions.

For the $(n;n'\gamma)$ case the type of transition sequence is:

$$J_0\,(j_1 = \ell_1 \pm 1/2)\; J_1\; (j_2 = \ell_2 \pm 1/2)\; J_2\; (L\; L')\; J_3$$

where:

J_0 initial spin of the target nucleus

j_1 total angular momentum of the incoming neutron

j_2 total angular momentum of the secondary neutron

J_1 spin of the compound nucleus

J_2 final spin of the excited target nucleus

J_3 final spin of the target nucleus

L ; $L' = L+1$ multipole orders of gamma radiation

ℓ_1 orbital angular momentum of the incoming neutron

ℓ_2 orbital angular momentum of the secondary neutron

The angular distribution of the gamma-ray transition $J_2(LL')J_3$ is[16]

$$\frac{d\sigma}{d\Omega} = \frac{\lambda^2(2J_1+1)^2(2J_2+1)}{8(2J_0+1)} \sum_{J_1 J_2, \nu} A\ B\ C\ D(\delta)\ \tau\ P_\nu(\cos\vartheta)$$

the summation is restricted to

$$0 \leq \nu \leq 2\ j_1,\ 2J_1,\ 2J_2,\ 2L'$$

and

$$A = (-1)^{J_0+J_3-j_2+1/2}(2j_1+1)$$

$$B = \langle \nu 0 | j_1 j_1 1/2 -1/2 \rangle$$

$$C = W(J_1 J_1 j_1 j_1 ; \nu J_0) W(J_1 J_1 J_2 J_2 ; \nu\ j_2)$$

$$\tau = \frac{T_{\ell_1}(E_1)\ T_{\ell_2}(E_2)}{\sum_{\ell jE} T_\ell(E)}$$ Hauser-Feshbach penetrability term

λ rationalized wavelength of the incident neutron in the center of mass system (c.m.s.)

$$D(\delta) = (1+\delta^2)^{-1}\ [D(LL)+2D(LL')\delta+\delta^2(L'L')]$$

where

$$D(LL') = (2L+1)^{1/2}(2L'+1)^{1/2} \langle \nu 0 | LL'1-1 \rangle\ W(J_2 J_2 L\ L' ; \nu J_3)$$

E_1 incident neutron energy in the c.m.s.

E_2 emergent neutron energy in the c.m.s.

ϑ angle of emergence referred to the incident neutrons beam direction

δ mixing ratio

When in a $(n;n'\gamma-\gamma)$ process the second gamma-ray of the cascade is observed and this radiation links the two levels of spin J_3 and J_4 respectively with multipolarities L_2, L_2' (the first gamma-ray linking the levels with the spins J_2 and J_3 has multipolarities L_1 and L_1') the tran

sition sequence is:

$$J_0\,(j_1=\ell_1\pm{}^1\!/_2)\;J_1\,(j_2=\ell_2\pm{}^1\!/_2)\;J_2(L_1L_1')\;\overset{\text{-observed-}}{J_3(L_2L_2')}\;J_4$$

The second gamma-ray angular distribution is now given by:

$$\frac{d\sigma}{d\Omega} = \frac{\lambda^2(2J_1+1)^2(2J_2+1)(2j_3+1)}{8(2J_0+1)} \sum_{j_1\,j_2\,\nu} E\;B\;C\;F(\delta_1)D(\delta_2)\,\tau\,P_\nu(\cos\vartheta)$$

the summation is restricted in this case to

$$0 \le \nu \le 2j_1, 2J_1, 2J_2, 2L_3', 2J_3$$

and

$$E = (-1)^{J_0-J_4-j_2+{}^1\!/_2}(2j_1+1)$$

$$F(\delta_1) = (1+\delta_1^2)^{-1}[F(L_1L_1)+\delta_1^2F(L_1L_1')]$$

and now

$$D(L_2L_2') = (2L_2+1)^{1/2}(2L_2'+1)^{1/2}\langle\nu 0|\,L_2L_2'1{-}1\rangle\;W(J_3J_3L_2L_2';\;\nu J_4)$$

In this work for spins and multipole mixing ratios determination purposes, the relative angular distribution $\frac{d\sigma/d\Omega|_\vartheta}{d\sigma/d\Omega|_{90^\circ}}$ of the investigated gamma-rays has been compared with the experimental one. The value at 90° for the experimental angular distributions has been determined using, for the experimental points, the same normalization constant as for the best fit curve. By this procedure the error of the 90° experimental point is not propagated to the other points. Comparing the relative angular distributions, the discrepancies between the theoretical and experimental differential cross sections or excitation function values, are not included in the determinations. This procedure has been adopted considering that for the energy region where the number of the open channels is small, the excitation function values predicted by the Hauser-Feshbach theory, are bigger than those given by the experiment.

This theory, however, is oversimplified especially in the treatment of compound nuclear resonances. Dresner ([21]), Lane and Lynn([22]) and Moldauer ([18, 20, 23]) proposed a level width fluctuation correction. Moldauer discussed also the resonance interference effect in the compound process. If the number of open channels is small, as in low energy neutron scattering, these corrections are important. It is well known in this case, that the width fluctuation correction lead to a decrease of the inelastic

cross section.

In the present work the gamma-ray excitation functions from neutron inelastic scattering, measured from 1 MeV to 4 MeV, were analysed by the use of the optical and statistical models. In these analysis, the aforesaid corrections were applied to the theoretical data.

In the calculations, two groups of neutron transmission coefficients have been employed for the computation of the Hauser-Feshbach term τ. The first group is obtained by using the local optical potential of Bjorklund and Fernbach ([24]), the second by using the non-local optical potential of Perey and Buck ([25]).

4. - RESULTS AND DISCUSSION

Excitation funtions.

The excitation functions for the predominant transitions from the first four levels of Fe^{56} are shown in Fig. 1 and Fig. 2. Our experimental points in the investigated energy interval are compared with the results of the other laboratories and with the theoretical previsions of the statistical theory and the corrections obtained considering the width fluctuation effects. The theoretical excitation functions reported in these and in the next figures, are calculated for the incoming neutron energy sequence: 1,0 MeV; 1,5 MeV; 2,0 MeV; 2,5 MeV; 3,0 MeV and 4,0 MeV. The curves between these points are reported only for eye guidance and cannot be exact at intermediate energies.

The numerical values of the cross sections are reported in Table 1. From the gamma-rays cross sections is possible to obtain the neutron inelastic cross sections, summing the cross sections for all gamma-rays originating at a given level and subtracting from this value the cross sections for all cascades to the given level. This procedure is adopted to obtain from our experimental data the inelastic neutron excitation functions of Fig. 3 and the numerical values of Table 2. In Fig. 3 these results are compared with some inelastic neutrons data of the literature and the theoretical previsions.

Gamma-rays relative angular distributions.

The relative angular distributions compared with the theoretical

data obtained using the two groups of neutron penetrabilities and the formulas of Par. 3 are reported from Fig. 5 to Fig. 11.

The calculated angular distributions include computation for all observed cascade contributions from higher levels. Experimental angular distributions for gamma-rays originating from levels whose spins and parities are unknown, were calculated with a number of the more likely spin and parity possibilities.

The decay scheme of Fe^{56} is shown in Fig. 4. It is based on the results of the present work and on the most recent $(p;p'\gamma)$, $(n;n'\gamma)$ as yet Co^{56} and Mn^{56} decay measurements.

- Decay modes.

The 0.846 MeV level 2^+ E_γ = 0.84 MeV.

The energy of this level has been determined using a curved crystal monochromator as 846.79±0.1 keV [26]. The spin and parity of this level have been established [27] as 2^+ [11, 28, 29, 30]. The decay to the ground state 0^+ can go only by a pure E2 transition as shown in Fig. 5, where the experimental gamma-ray distributions of present measurements are compared with the E2 theoretical angular distributions from 1.0MeV to 4.0 MeV for the incident neutron energy.

The cross section values given by Hauser-Feshbach theory are in disagreement with the experimental data for the energy values between the threshold and about 2 MeV above threshold energies.

The excitation functions given for the two set of neutron penetrabilities by Moldauer's corrections are in better agreement than the pure statistical theory, as can be seen in Fig. 1.

The 2.085 MeV level 4^+ E_γ = 1.24 MeV.

The spin and parity of this level have been established as 4^+ [31]. In agreement with this assignment are the studies of the reactions $Fe^{56}(d;t)$; $Fe^{56}(\alpha;\alpha')$ [29, 30] and $Fe^{56}(n;n'\gamma)$ [11]. The 2.085 MeV level decays to the first 0.846 MeV level via an E2 transition. The comparison of the theoretical angular distributions with the experimental points agree with this decay mode as can be seen in Fig. 6. Also the experimental and theoretical excitation functions are in good agreement.

The 2.656 MeV level 2^+ E_γ = 1.81 MeV E_γ = 2.66 MeV.

In these measurements we have observed only the 1.81 MeV transition to the first 0.846 MeV level. The branching ratios shown in Fig. 4 are from the $Fe^{56}(p;p'\gamma)$ measurements of Hinrichsen ([7]). The spin and parity of the level have been well established ([27,32]). The mixing ratio δ of the 1.81 MeV gamma-ray from radioactivity measurements varies from 0,15 to 0,20 ([27]), while in $Fe^{56}(p;p'\gamma)$ angular distributions ([7]) a value of 0,15± ±0,04 has been obtained.

In Fig. 7 our experimental angular distributions at 3.0 MeV and 4.0 MeV of incident neutron energies are compared with the theoretical curves for pure M1 and E2 transitions.

The mixed multipole curves give δ values of 0,16±0,04 and 0,12±0,04 respectively.

The 2.941 MeV level E_γ = 2.09 MeV.

This gamma-ray are not resolved from the gamma radiation linking the 2.960 MeV level with the 0.846 MeV level, but the contribution to this gamma-ray is less than 10%.

The 2.960 MeV level 2^+ E_γ = 2.12 MeV E_γ = 2.96 MeV.

The spin assignment for this level is well established. Only the transition with E_γ = 2.12 MeV to the 0.846 MeV level is observed. As in the $Fe^{56}(n;n'\gamma)$ measurements of Benjamin ([11]) the comparison of our experimental results of Fig. 8 with the theoretical angular distributions show an almost pure M1 transition.

The value of the mixing ratio from radioactivity measurements ([27]) is 0,28.

The 3.120 MeV ($1^\pm$; $3^\pm$) and the 3.132 MeV 4^+ doublet E_γ = 1.03 MeV E_γ = 2.27 MeV E_γ = 3.12 MeV.

The level at 3.120 MeV decays to the 0.846 MeV 2^+ state via a 2.27 MeV gamma-ray and to the 0^+ ground state via a 3.12 MeV gamma-ray. The spin of the level at 3.120 MeV is limited to 0^+ $1^\pm$ $2^\pm$ or 3^- by the absence of a branch to this level in the decay of Co^{56} (log ft value ≥ 9). The upper 3.123 MeV member of the doublet decays predominantly to the 2.085 MeV 4^+ state via a 1.03 MeV gamma-ray.

For the level at 3.123 MeV populated by the decay of the Co^{56}, log ft = = 7, which limits the possible spin assignments for this level to 3, 4 or 5.

The proton angular distributions from the $Fe^{54}(t;p)$ reaction [28] show a level of spin 5, while $Fe^{56}(\alpha;\alpha')$ measurements [7] show a level of spin 4^+ at this energy. In Fig. 9 our experimental data for the 2.27 MeV gamma-ray angular distributions are compared with the aforesaid spin possibilities at 3.5 MeV of source neutrons. This comparison eliminate two of the aforesaid spin possibilities (0^+ and $2^\pm$), but is unable to choose between $1^\pm$ or 3^-. Multipolarity considerations seem to prefer the 3^- state, but this is not a decisive argument.

The comparison of the angular distributions of 1.03 MeV gamma-ray in Fig. 10 gives for the 3.123 MeV member of the doublet the spin value of 4. From the exitation function at 3.5 MeV and 4.0 MeV of neutron energies, the parity of this level is established as even.

The 3.369 MeV level 2^+ E_γ = 2.52 MeV E_γ = 3.37 MeV.

The angular distributions of Fig. 11 at 3.5 MeV and 4.0 MeV show a 2^+ state for this level.

The 2.52 MeV transition appears to be mostly M1. This gamma-ray has been seen in $(n;n'\gamma)$ measurements of Armitage et al. [12]. The 2^+ spin value determined from angular distributions of Fig. 11 is consistent with the assignment from $Fe^{54}(t;p)Fe^{56}$ reaction of Cohen and Middleton [28] and with the measurements of nuclear alignment of Diddens et al. [9].

The 3.444 MeV and 3.447 MeV 1 doublet E_γ = 0.79 MeV E_γ = 1.36 MeV E_γ = 2.60 MeV E_γ = 3.45 MeV.

When the decay scheme of Fig. 4 is adopted, only the E_γ = 3.45 MeV angular distribution can give informations on the state of a member of the doublet in this measurements. In fact the E_γ = 2.60 MeV decay mode from the 3.45 MeV doublet to the first 0.846 MeV levels is common for the two members.

For the E_γ = 1.36 MeV reliable angular distributions could not be obtained, because in these measurements natural iron sample has been used, the Fe^{54} E_γ = 1.41 MeV transition obscures that of the 1.36 MeV gamma-ray. Analogous situation for the E_γ = 0.79 MeV with respect to the

0.846 MeV gamma-ray transition for the first level of Fe^{56}.

The angular distributions obtained for the E_γ = 3.45 MeV gamma-ray at 4.0 MeV of incident neutron energy are reported in Fig. 11.

The 1^+ state pure M1 transition obtained in our measurements for the upper level is consistent with the assignment derived from the $(n;n'\gamma)$ measurements of Benjamin et al.([11]) and from the $(p;p'\gamma)$ measurements of Hinrichsen et al.([7]).

The 3.600 MeV and 3.605 MeV 2^+ doublet $E\gamma$ = 2.76 MeV $E\gamma$ = 3.60 MeV.

The considerations on the 2.60 MeV gamma-ray of the foregoing doublet are valid for the present $E\gamma$ = 2.76 MeV. Then only the $E\gamma$ = 3.60 MeV angular distribution can be considered for spin and parity determination with the resolution given by our spectrometer.

The comparison of the experimental and theoretical values obtained for the 3.60 MeV gamma-ray shown in Fig. 8 is consistent with a 2^+ state for the lower member of the doublet. This assignment is consistent with that of $(n;n'\gamma)$ measurements of Benjamin et al.([11]) and is supported by the $Fe^{56}(\alpha;\alpha')$ ([30]) and by $(p;p'\gamma)$ data ([7]).

The spin and parity assignments derived from this and other laboratories measurements are resumed in Table 3.

5. - CONCLUDING REMARKS

Combining the experimental informations obtained by Ge(Li) spectrometers on the nuclear levels or doublet members energy positions with the angular distributions and cross sections informations given by a NaI(Tℓ) time-of-flight spectrometer and the Satchler-Sheldon theoretical previsions, informations can be gained on unknown or not well determinated nuclear states. The results of this investigation on Fe^{56} nucleus and the informations gained for the 3.12 MeV; 3.40 MeV; 3.60 MeV doublets are certainly an evaluation of the method.

Experiments and data evaluation of this kind, now in progress in this laboratory on other nuclei, should help to eliminate some uncertainties on spin and parity assignments.

T A B L E 1

Experimental (n;n'γ) isotopic cross sections (mb) for Fe^{56}.

E_γ (MeV)	E_n (MeV)						
	1.0	1.5	2.0	2.5	3.0	3.5	4.0
0.846	282±29	702±71	767±77	924±93	1122±112	1405±140	1181±118
1.03							62±6
1.24				32±4	128±13	178±18	196±20
1.81					207±21	273±28	181±19
2.12						220±23	167±17
2.27						150±16	106±11
2.52						45±5	38±4
2.60							76±8
2.76							15±2
3.45							52±6
3.60							57±7

TABLE 2

Inelastic neutron isotopic cross sections (mb) for Fe^{56}.

E_{level} (MeV)	E_n (MeV)						
	1.0	1.5	2.0	2.5	3.0	3.5	4.0
0.846	282±29	702±71	767±77	892±93	787±115	522±147	426±124
2.085				32±4	128±13	178±18	134±21
2.656					207±21	273±28	181±26
2.960						224±23	170±18
3.120						155±16	109±12
3.123							62±6
3.369						54±6	45±5
3.44 d							143±22
3.60 d							72±13

d doublet

TABLE 3

Spin and parity assignments for Fe^{56}.

E_{level} (MeV)	a	b	c	d	e	f	g	h	i
0.846	2^+	2^+	2^+		2^+	2^+	2^+	2^+	2^+
2.085	4^+	4^+		4^+	4^+	4^+	4^+	4^+	4^+
2.656	2^+	2^+	(2^+)		2^+	2^+	2^+	2^+	2^+
2.940		6^+					0^+	0^+	
2.960	2^+	2^+		2^+	2^+	2^+	2^+	2^+	2^+
3.120								$(0^+1^+2^+)$	(1;3)
3.123	$3^+(4^+;3^-)$	2^+	3^-	4^+	$(3^-$:1 or 2) doublet	(4^+)	5^-	$(3^+4^+5^+)$	4^+
3.369		3^+					2^+		2^+
3.386		5^+							
3.444	$(3^+;3^-)$	2^+	3^-		3^+	3^+	not 1^-	$(2^+;3^+)$	
3.447					1^+		not 1^-	$(1^+;2^+)$	1^+
3.600		4^+			2^+		0^+	$(1^+;2^+)$	
3.605								$(0^+1^+2^+)$	2^+

a) Metzger ([35]) Mn^{56} beta decay and Poppema et al. ([31]) Co^{56} beta decay.
b) Gilboy et al. ([1]) inelastic neutron scattering.
c) Ricci et al.([36]) 155 MeV inelastic proton scattering.
d) Benjamin et al.([11]) (n;n'γ) measurements.
e) Matsuda ([37]) 14.65 MeV inelastic proton scattering.
f) Armitage et al.([12]) (n;n'γ) and Co beta decay.
g) Cohen et al.([28]) Fe^{54} (t;p) Fe^{56}
h) Hendrie et al.([31]) inelastic alfa scattering.
i) This measurement.

The parities and the spin values enumerated on the table are only those directly deduced from the measurements of each reference.

REFERENCES

(1) W.B. Gilboy and J.H. Towle - Nucl. Phys. 64 (1965) 130.

(2) A. Sperduto and W.W. Buechner - Phys. Rev. 134 (1964) B 142.

(3) A. Aspinall, B. Brown and S.E. Warren - Nucl. Phys. 46 (1963) 33.

(4) M.H. Saphiro, P.F. Hinrichsen, R.Middleton and R.K. Mohindra - Phys. Lett. 19 (1965) 573.

(5) J.R. Macdonald and M.A. Grace - Nucl. Phys. A92 (1967) 593.

(6) G. Brown, S.E. Warren and R. Middleton - Nucl. Phys. 77 (1966) 365.

(7) P.F. Hinrichsen, M.H. Saphiro and D.M. Van Patter - Nucl. Phys. A101 (1967) 81.

(8) A.A. Kabsanos, J.R. Huitzenga and H.K. Vonach - Phys. Rev. 141 (1966) 1053.

(9) A.N. Diddens, W.J. Huiskamp, J. C. Severiens, A.R. Miedema and M.J. Steenland - Nucl. Phys. 5 (1958) 58.

(10) P. Kienle and R.E. Segel - Phys. Rev. 114 (1959) 1554.

(11) R.W. Benjamin, P.S. Buchanan and I.L. Morgan - Nucl. Phys. 79 (1966) 241.

(12) B.H. Armitage, A.T. Ferguson and G.C. Neilson - Nucl. Phys. A133 (1969) 241.

(13) G.R. Satchler - Phys. Rev. 94 (1954) 1304.

(14) G.R. Satchler - Phys. Rev. 104 (1956) 1198.

(15) G.R. Satchler - Phys. Rev. 111 (1958) 1747.

(16) E. Sheldon and D.M. Van Patter - Rev. Mod. Phys. 38 (1966) 143.

(17) W. Hauser and H. Feshbach - Phys. Rev. 87 (1952) 366.

(18) P.A. Moldauer - Phys. Rev. 123 (1961) 968.

(19) P.A. Moldauer - Phys. Rev. 129 (1963) 754.

(20) P.A. Moldauer - Rev. Mod. Phys. 36 (1964) 1079.

(21) L. Dresner - Proc. Int. Conf. on neutron interaction with the nucleus, Columbia University Report CU-175 (1957) p. 71.

(22) A.M. Lane and J.E. Lynn - Proc. Phys. Soc. A 70 (1957) 77.

(23) P.A. Moldauer - Phys.Rev. 135 (1964) B642.

(24) F. Bjorklund and S. Fernbach - Phys. Rev. 109 (1958) 1296.

(25) F. Perey and B. Buck - Nucl. Phys. 32 (1962) 353.

(26) J.J. Reidy and M.L. Wiedenbeck - Nucl. Phys. 70 (1965) 718.

(27) K. Way et al. Nuclear data Sheets (National Academy of science - National Research Council. Washington, D.C.)

(28) B.L. Cohen and R. Middleton - Phys. Rev. 146 (1966) 748.

(29) J. Kremenk and W.W. Daenik - Bull. Am. Phys. Soc. 11 (1966) 99.

(30) D.L. Hendrie, J. Valentin, I. Gabrielli, J. Mahoney and J. R. Meriwether - Bull. Am. Phys. Soc. 11 (1966) 351.

(31) O.J. Poppema et al. - Physica 21 (1955) 223.

(32) P. Dagley, M.A. Grace, J.M. Gregory and J.S. Hill - Proc. Roy. Soc. 250A (1955) 550.

(33) H. Petterson, O. Bergmann and C. Bergman - Ark. Fys. 29 (1965) 423.

(34) R. Day - Phys. Rev. 102 (1956) 767.

(35) F.R. Metzger and W.B. Tott - Phys. Rev. 92 (1953) 904.

(36) R.A. Ricci, J. Jacmart, M. Lin, M. Rion and C. Ruhla - Nucl. Phys. A91 (1967) 609.

(37) K. Matsuda - Nucl. Phys. 33 (1962) 536.

(38) J.J. Hopkins and M.G. Silbert - Nucl. Sci. Eng. 19 (1964) 431.

(39) V.E. Scherrer, B.A. Allison and W.R. Faust - Phys. Rev. 96 (1954) 386.

(40) J.H. Montague and E.B. Paul - Nucl. Phys. 30 (1962) 93.

(41) Shiroh Kikuchi, Kotoyuki Okano and Kazuaki Nishimura - JAERI 1078 (1965).

* * *

FIGURE CAPTIONS

Fig. 1 - 0.846 MeV gamma-ray inelastic excitation functions. • present measurements. o Benjamin et al.([11]). Δ Shiroh Kikuchi et al.([41]). ◇ Day ([34]).

———— Hauser-Feshbach calculations without width fluctuation correction. ------ Hauser-Feshbach calculations with width fluctuation corrections.

P.B. calculated using the non-local optical potential of Perey and Buck. B.F. calculated using the local optical potential of Bjorklund and Fernbach.

Fig. 2 - Experimental and theoretical excitation functions for gamma radiation from second, thirdh and fourth level of Fe^{56} in $(n;n'\gamma)$ reactions. • present measurements. o Benjamin et al.([11]). Δ Montague et al.([47]). ◇ Day ([34]). ▲ Scherrer et al.([39]). For the theoretical curves the notation of Fig. 1 has been used.

Fig. 3 - Experimental and theoretical neutron inelastic excitation functions for the first and the second level in Fe^{56} derived from gamma radiation data in these measurements (•); (o) Gilboy et al. ([1]) and (Δ) Hopkins et al. ([38]) data are from inelastic neutron scattering measurements. For the theoretical curves the notation of Fig. 1 has been used.

Fig. 4 - Decay scheme of Fe^{56}. The branchings are the weighted averages from studies of Co^{56}, Mn^{56} decay and $(p;p'\gamma)$ measurements ([7]). The energies are derived from Ge(Li) spectrometer measurements on Fe^{56} $(p;p'\gamma)$ ([7]), $Fe^{56}(n;n'\gamma)$ reactions and Co^{56} beta decay ([12]). Spin and parity assignments are derived from the present measurements.

Fig. 5 - The experimental and calculated relative angular distributions for the 0.846 MeV gamma-ray at several neutron energies (E_n). Curves are Satchler-Sheldon calculations with the penetrabilities of Bjorklund-Fernbach (———) and Perey-Buck (-----). Only relative errors have been represented.

Fig. 6 - The experimental and theoretical relative angular distributions for the 1.24 MeV gamma-ray from the second level of Fe^{56} at several neutron energies (E_n). For the theoretical curves the notation of Fig. 5 has been used.

Fig. 7 - Relative angular distributions for the 1.81 MeV gamma-ray from the 2.656 MeV 2^+ level of Fe^{56}. The theoretical distributions has been calculated with different mixing ratios. For the penetrabilities and errors see the notation of Fig. 5.

Fig. 8 - Relative angular distributions for the 2.12 MeV gamma-ray from the 2.960 MeV 2^+ level and for the 3.60 MeV gamma-ray from the 3.600 MeV 2^+ level of Fe^{56}. Penetrabilities and errors as in Fig. 5.

Fig. 9 - Comparison of the experimental relative angular distributions for the 2.27 MeV gamma-ray from the lower member of the 3.12 MeV doublet with the theoretical distributions calculated for some spin possibilities. For penetrabilities and errors see the notation of Fig. 5.

Fig. 10 - Experimental relative angular distributions for the 1.03 MeV gamma-ray from the upper member of the 3.12 MeV doublet compared with the theoretical distributions calculated for some spin possibilities. For the theoretical curves the notation of Fig. 5 has been used.

Fig. 11 - Relative angular distributions for the 2.52 MeV gamma-ray from the 3.369 MeV 2^+ level and for the 3.45 MeV gamma-ray from the upper 1^+ member of the 3.45 MeV doublet. For the theoretical curves and for errors see Fig. 5.

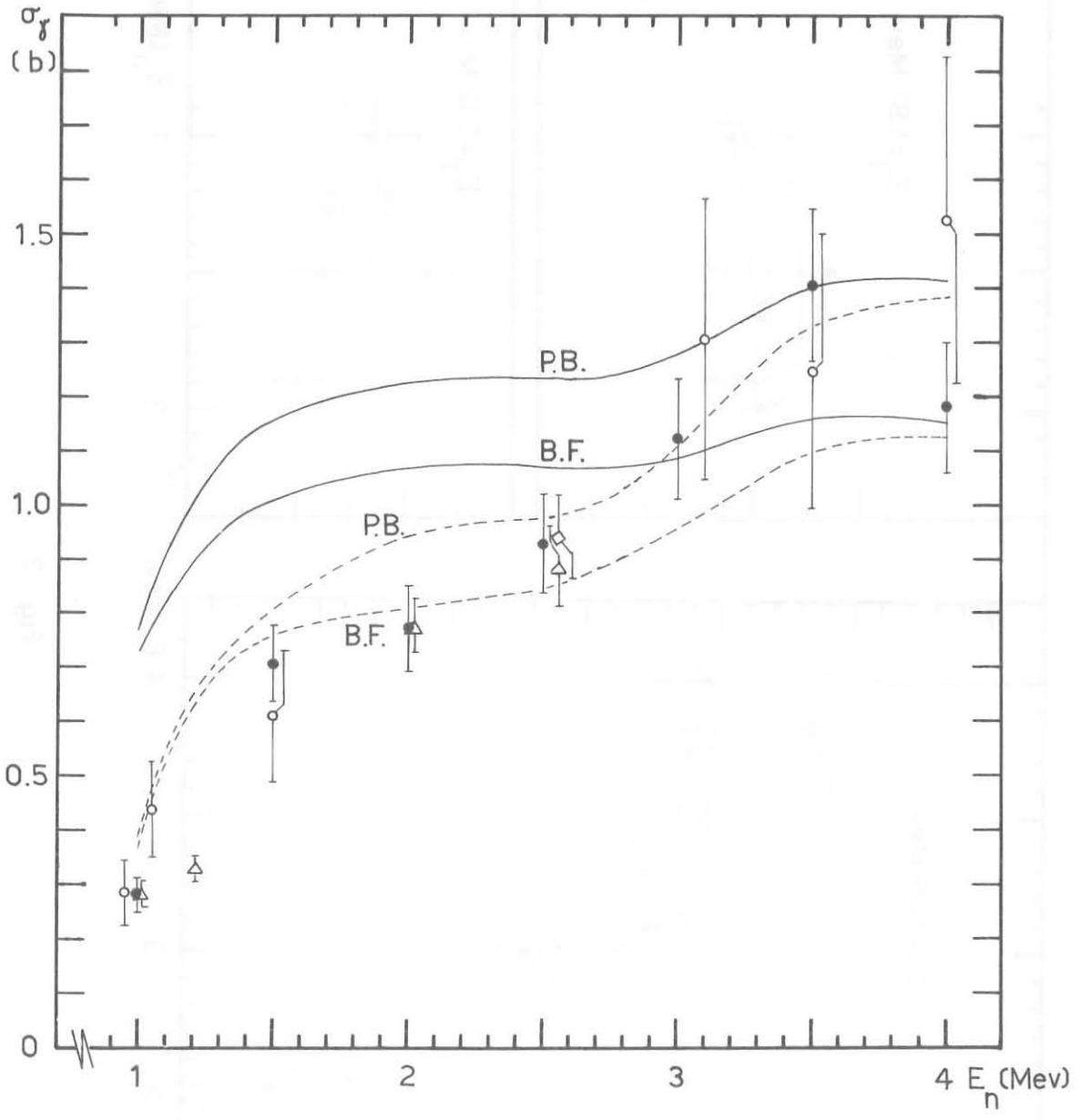

Fig. 1

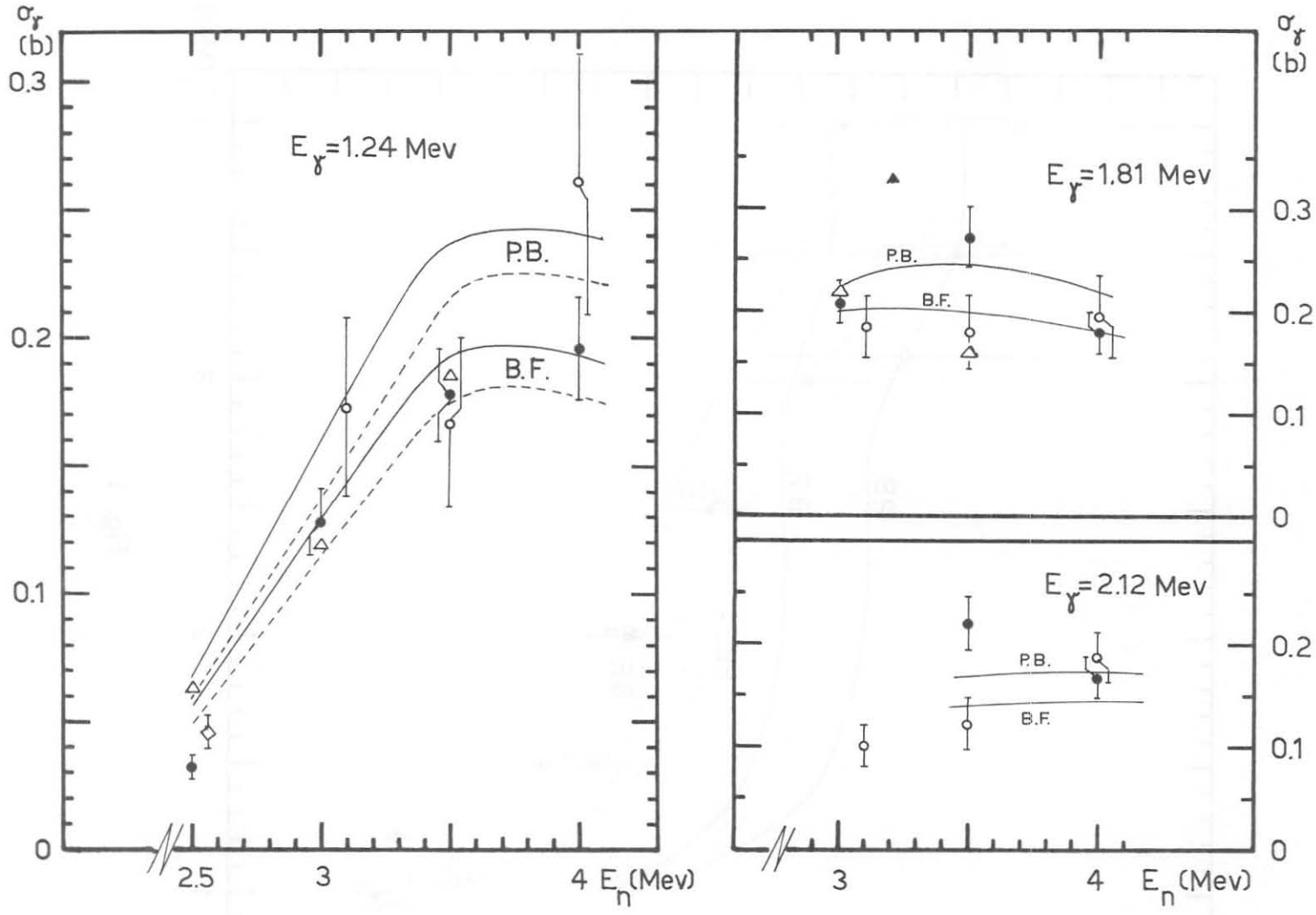
σγ (b)
0.3
0.2
0.1
0
Eγ=1.24 Mev
P.B.
B.F.
2.5
3
4 En(Mev)
Eγ=1.81 Mev
P.B.
B.F.
Eγ=2.12 Mev
P.B.
B.F.
3
4 En(Mev)

Fig. 2

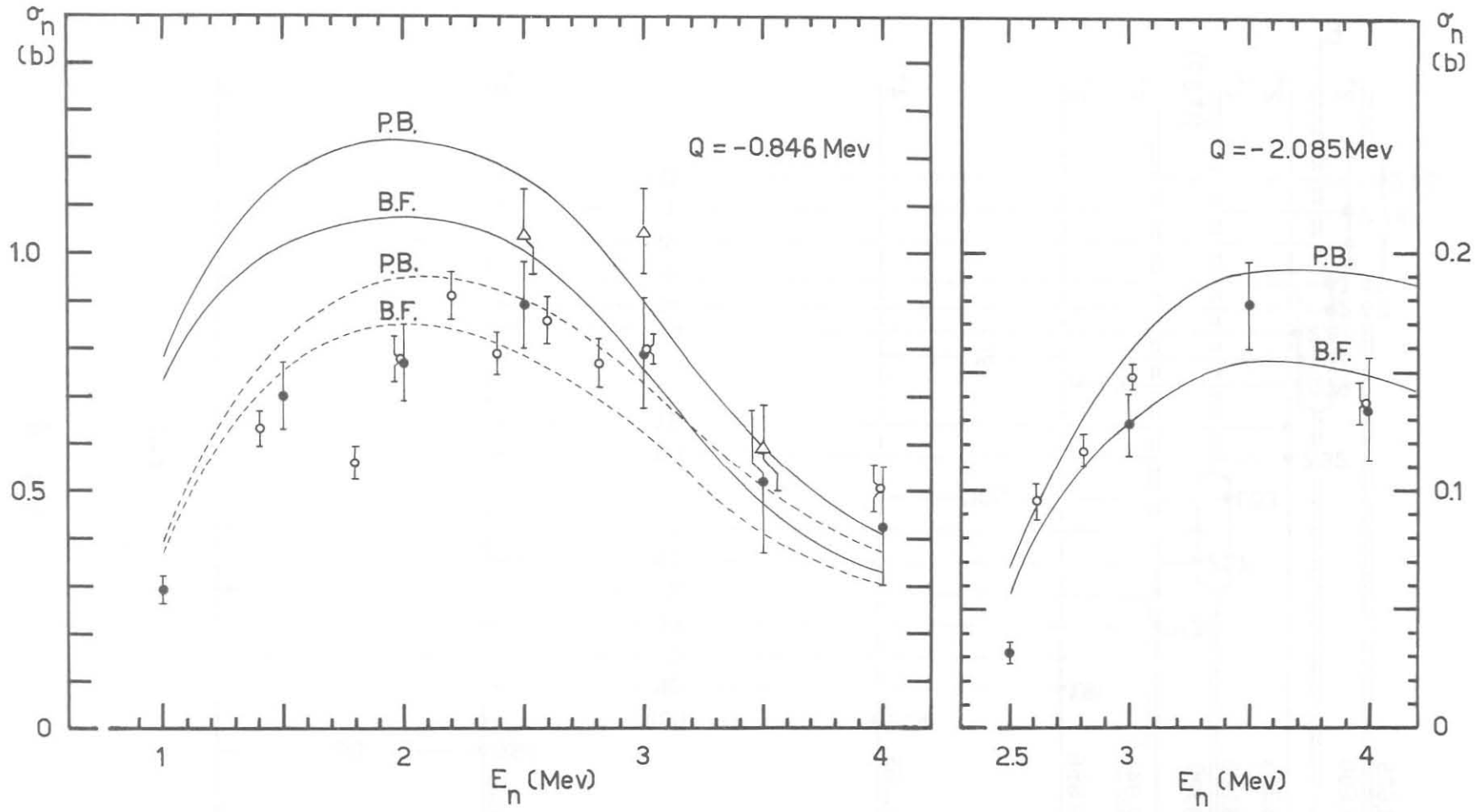
σn (b)
P.B.
B.F.
P.B.
B.F.
Q = −0.846 Mev
1.0
0.5
0
1
2
3
4
En (Mev)
σn (b)
Q = − 2.085 Mev
P.B.
B.F.
0.2
0.1
0
2.5
3
4
En (Mev)

Fig. 3

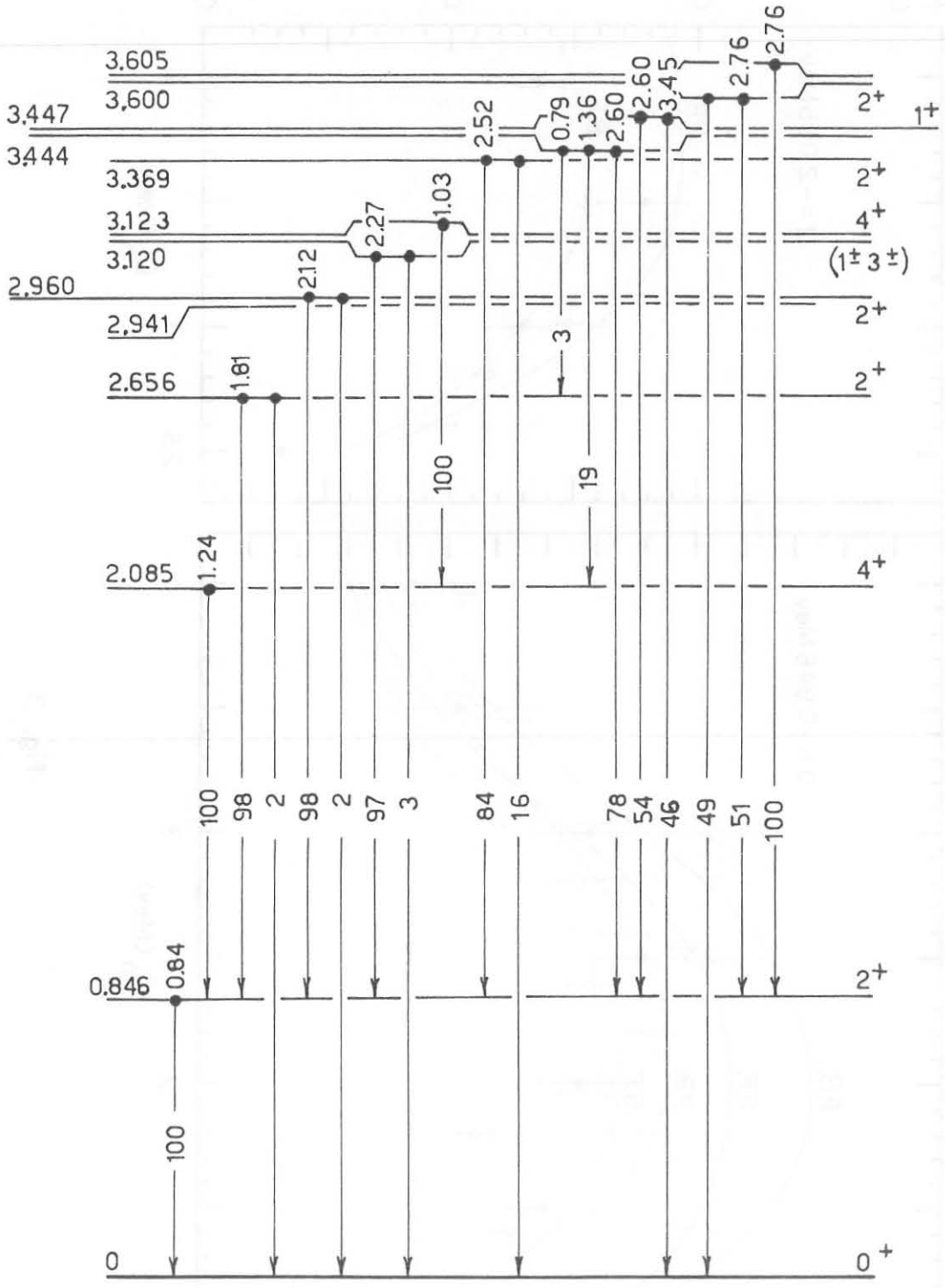
3.605
3.600
3.447
3.444
3.369
3.123
3.120
2.960
2.941
2.656
2.085
0.846
0
2.52
0.79
1.36
2.60
2.60
3.45
2.76
2.76
1.03
2.27
212
1.81
1.24
0.84
3
100
19
100
98
2
98
2
97
3
84
16
78
54
46
49
51
100
100
2+
1+
2+
4+
(1± 3±)
2+
2+
4+
2+
0+

Fe^{56}

Fig. 4

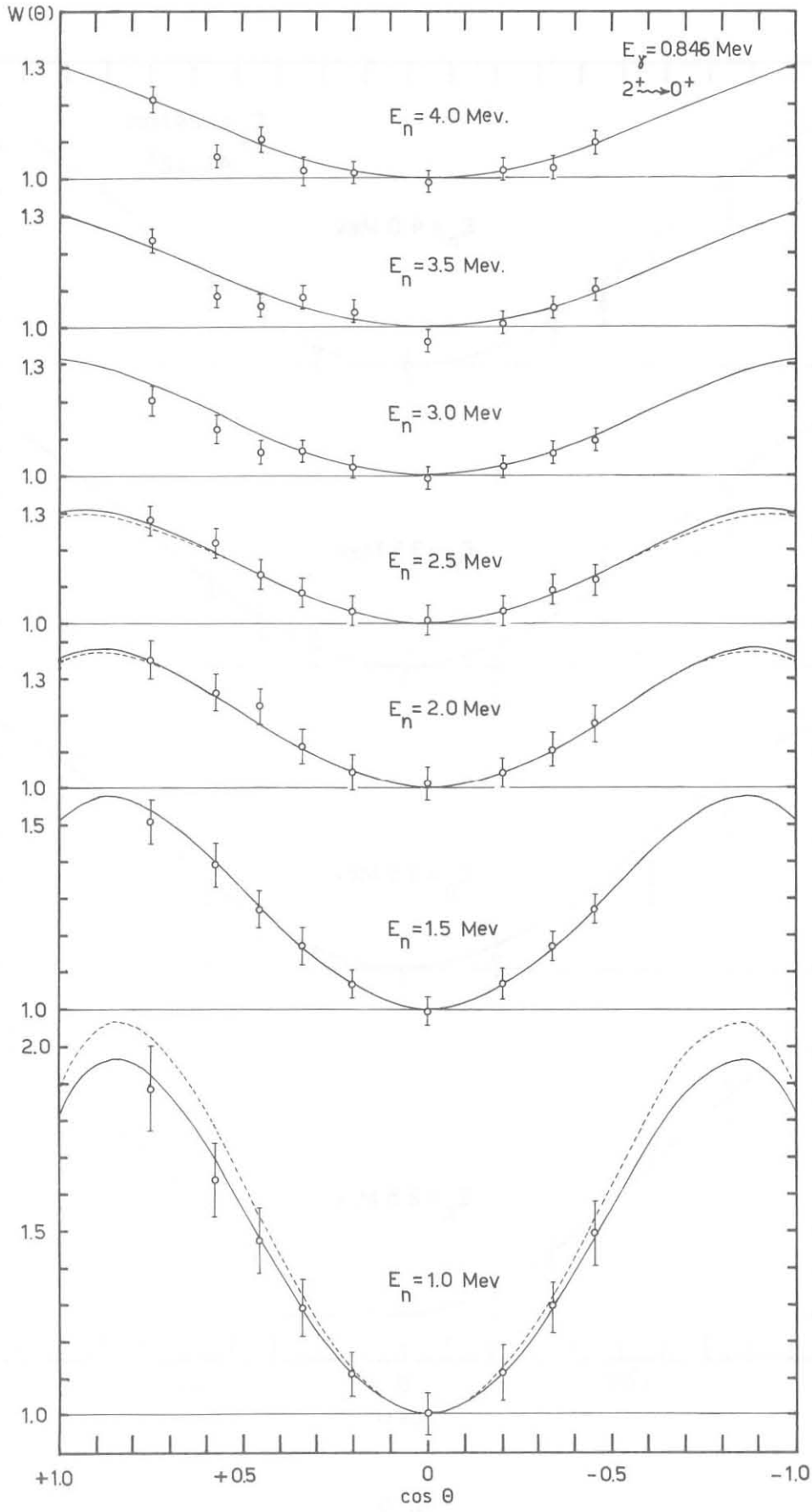
W(θ)
E_γ = 0.846 Mev
2+ → 0+
E_n = 4.0 Mev.
E_n = 3.5 Mev.
E_n = 3.0 Mev
E_n = 2.5 Mev
E_n = 2.0 Mev
E_n = 1.5 Mev
E_n = 1.0 Mev
1.3
1.0
1.5
2.0
+1.0
+0.5
0
-0.5
-1.0
cos θ

Fig. 5

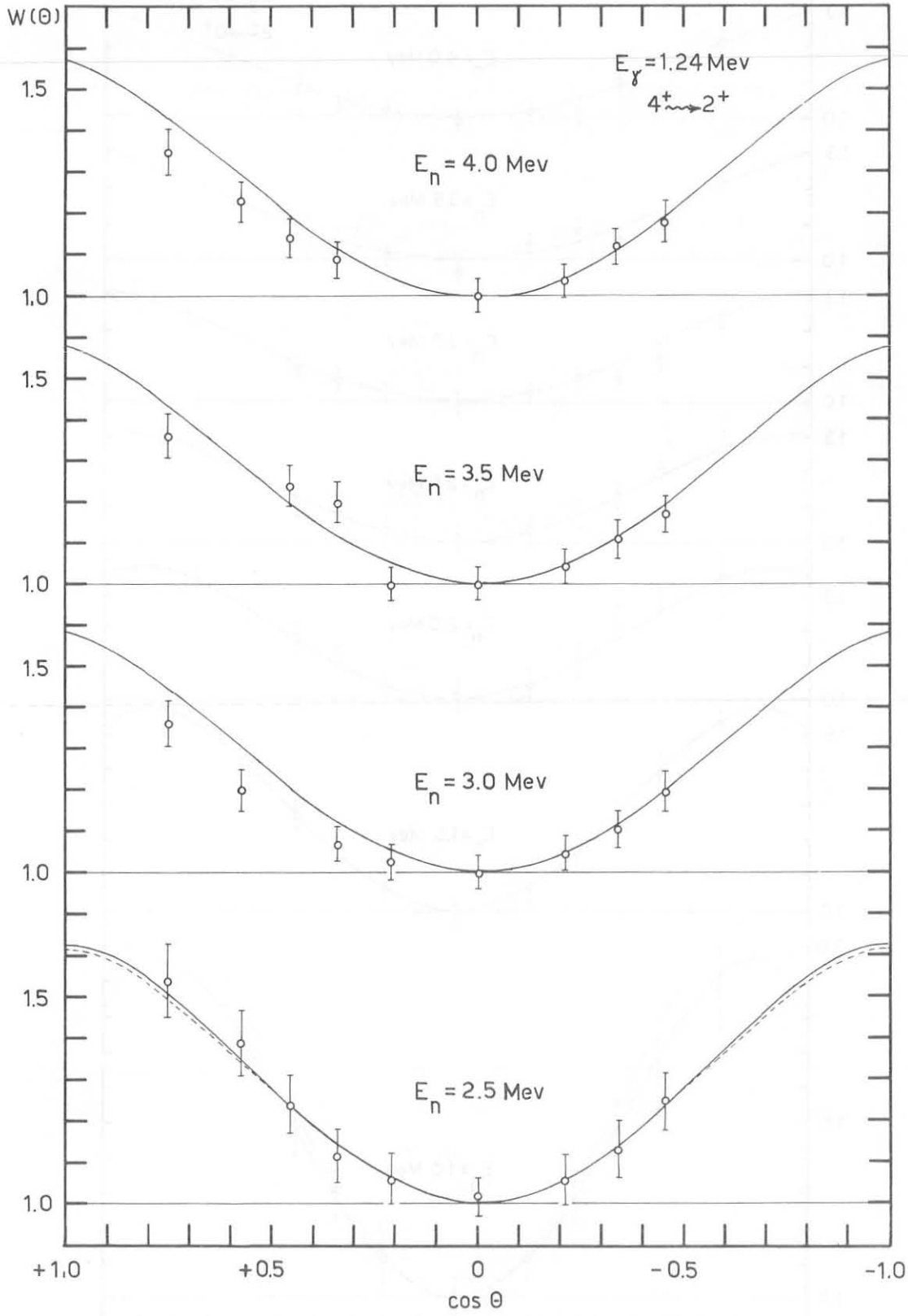
W(θ)
1.5
1.0
E_γ = 1.24 Mev
$4^+ \rightsquigarrow 2^+$
E_n = 4.0 Mev
E_n = 3.5 Mev
E_n = 3.0 Mev
E_n = 2.5 Mev
+1.0
+0.5
0
-0.5
-1.0
cos θ

Fig. 6

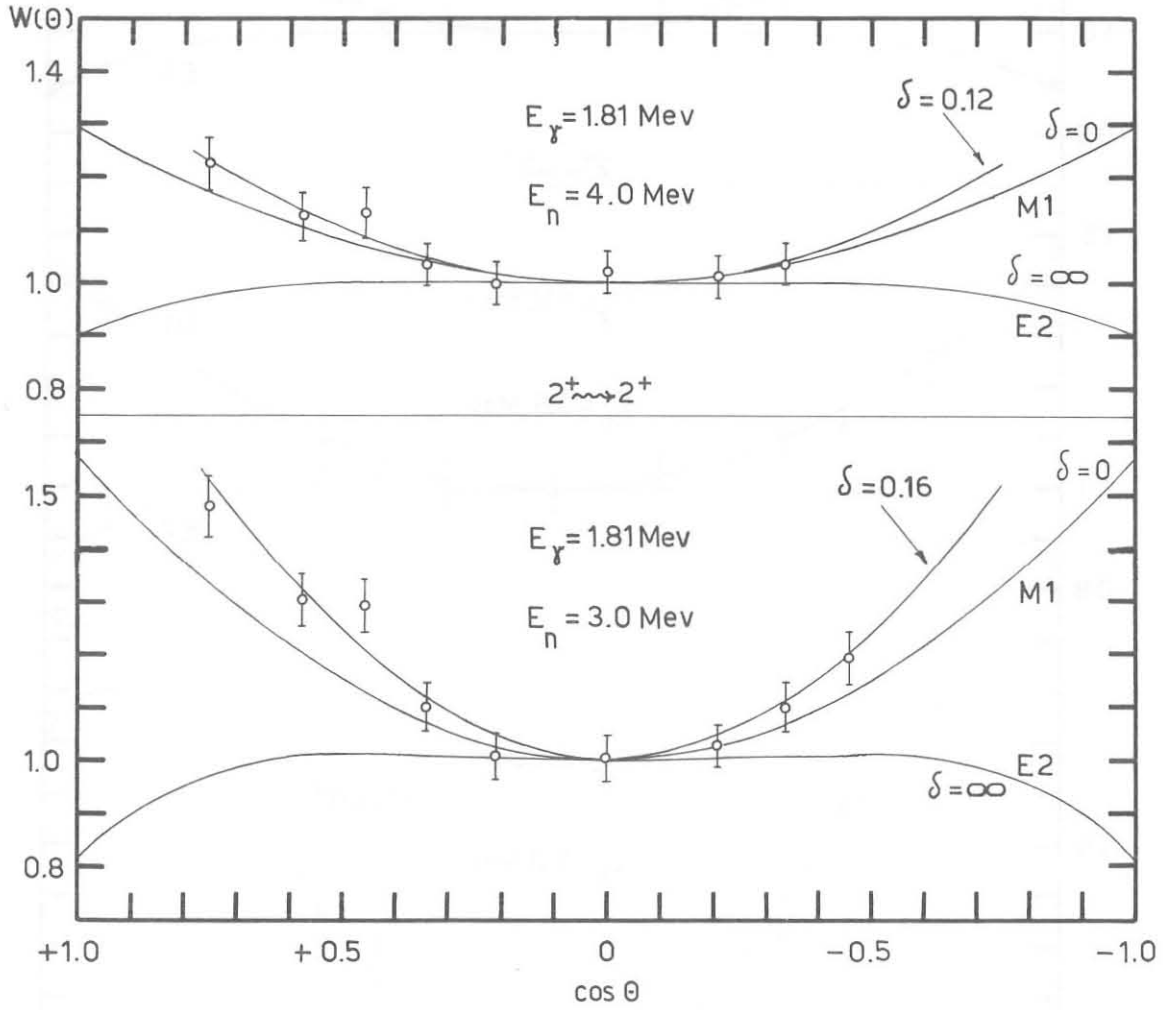
W(Θ)
1.4
1.0
0.8
E_γ = 1.81 Mev
E_n = 4.0 Mev
δ = 0.12
δ = 0
M1
δ = ∞
E2
2⁺ ⇝ 2⁺
1.5
1.0
0.8
E_γ = 1.81 Mev
E_n = 3.0 Mev
δ = 0.16
δ = 0
M1
E2
δ = ∞
+1.0
+ 0.5
0
−0.5
−1.0
cos Θ

Fig. 7

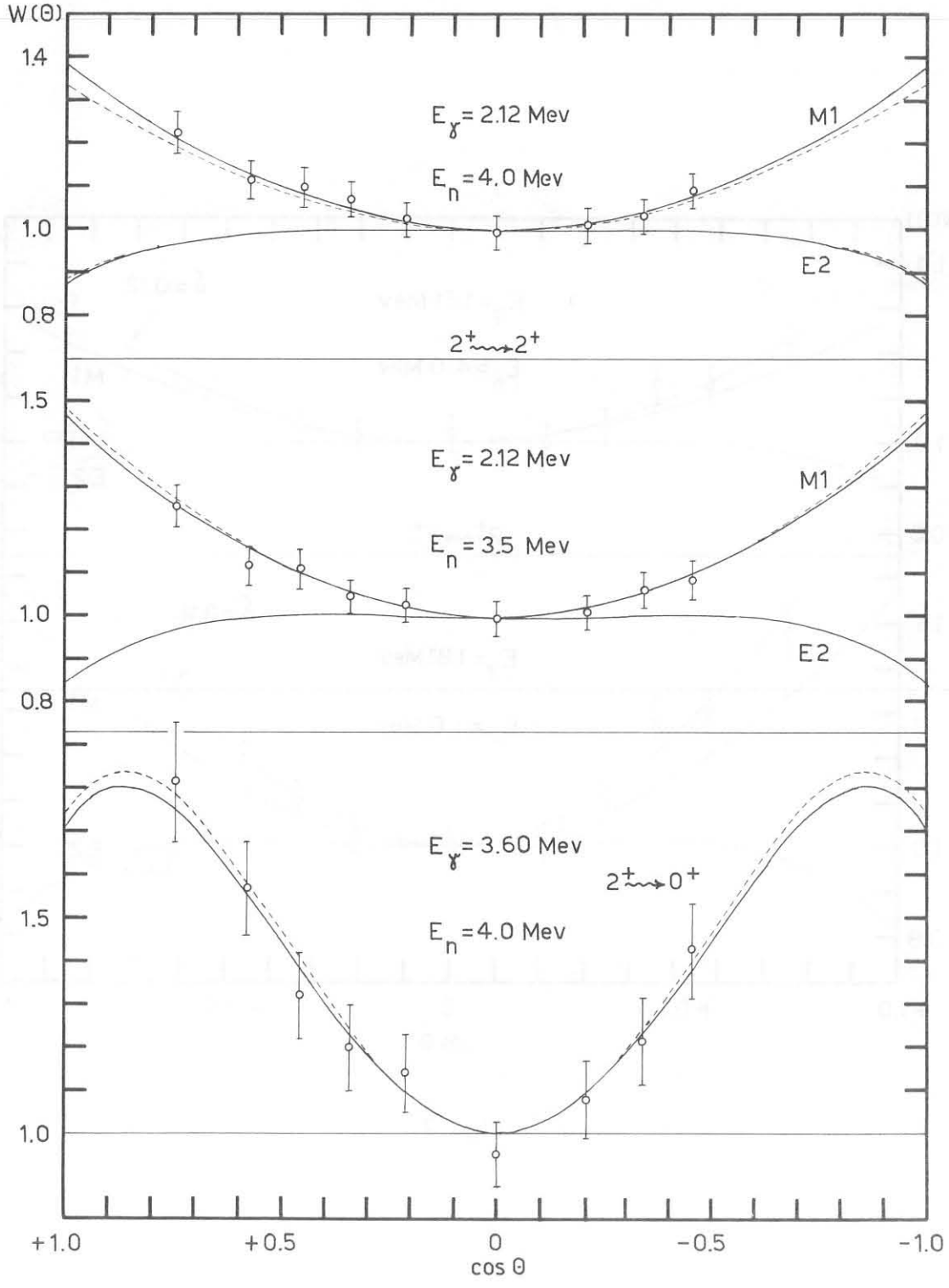
W(Θ)
1.4
1.0
0.8
E_γ = 2.12 Mev
E_n = 4.0 Mev
M1
E2
$2^+ \rightsquigarrow 2^+$
1.5
1.0
0.8
E_γ = 2.12 Mev
E_n = 3.5 Mev
M1
E2
1.5
1.0
E_γ = 3.60 Mev
$2^+ \rightsquigarrow 0^+$
E_n = 4.0 Mev
+1.0
+0.5
0
−0.5
−1.0
cos Θ

Fig. 8

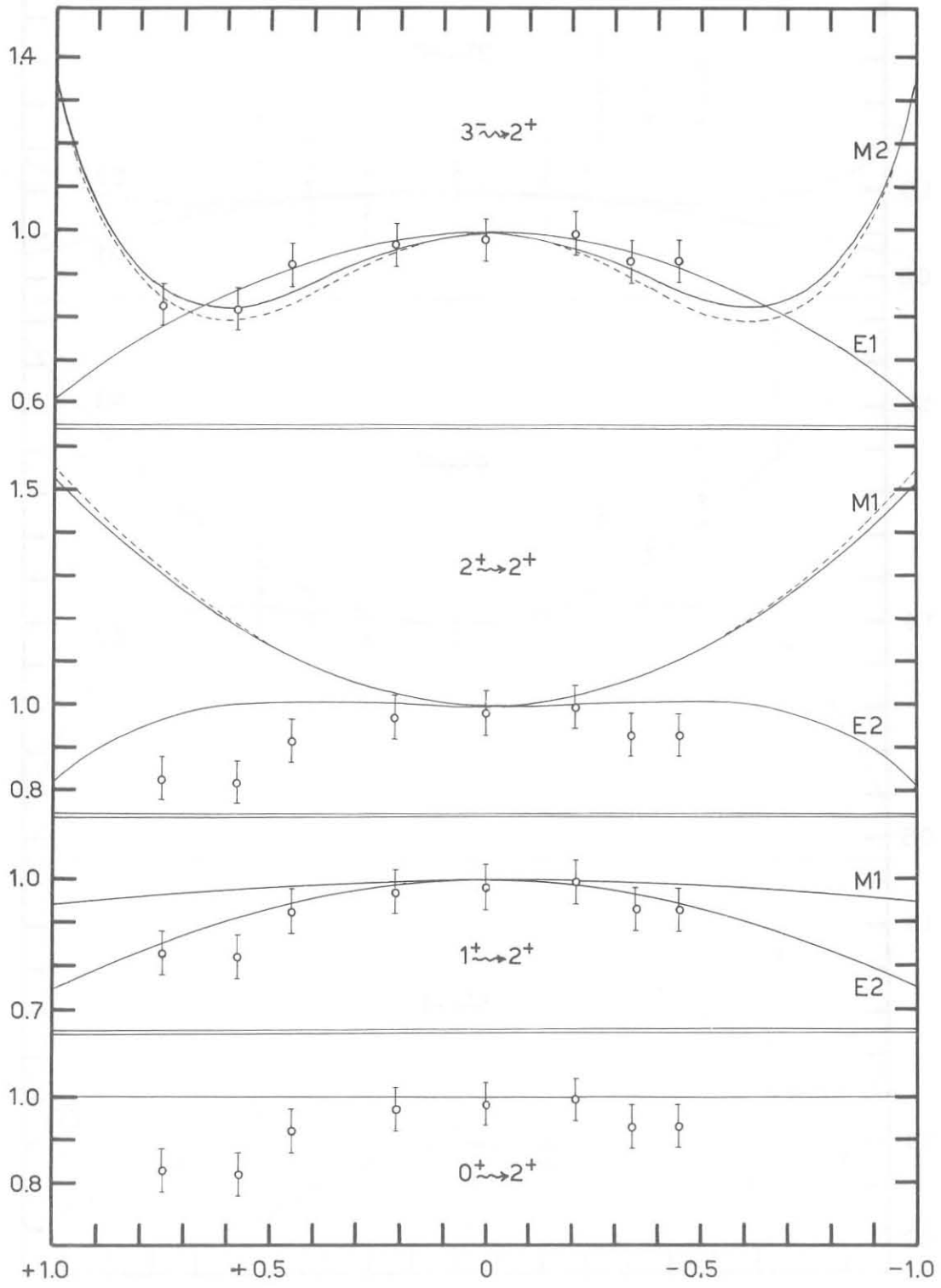

Fig. 9

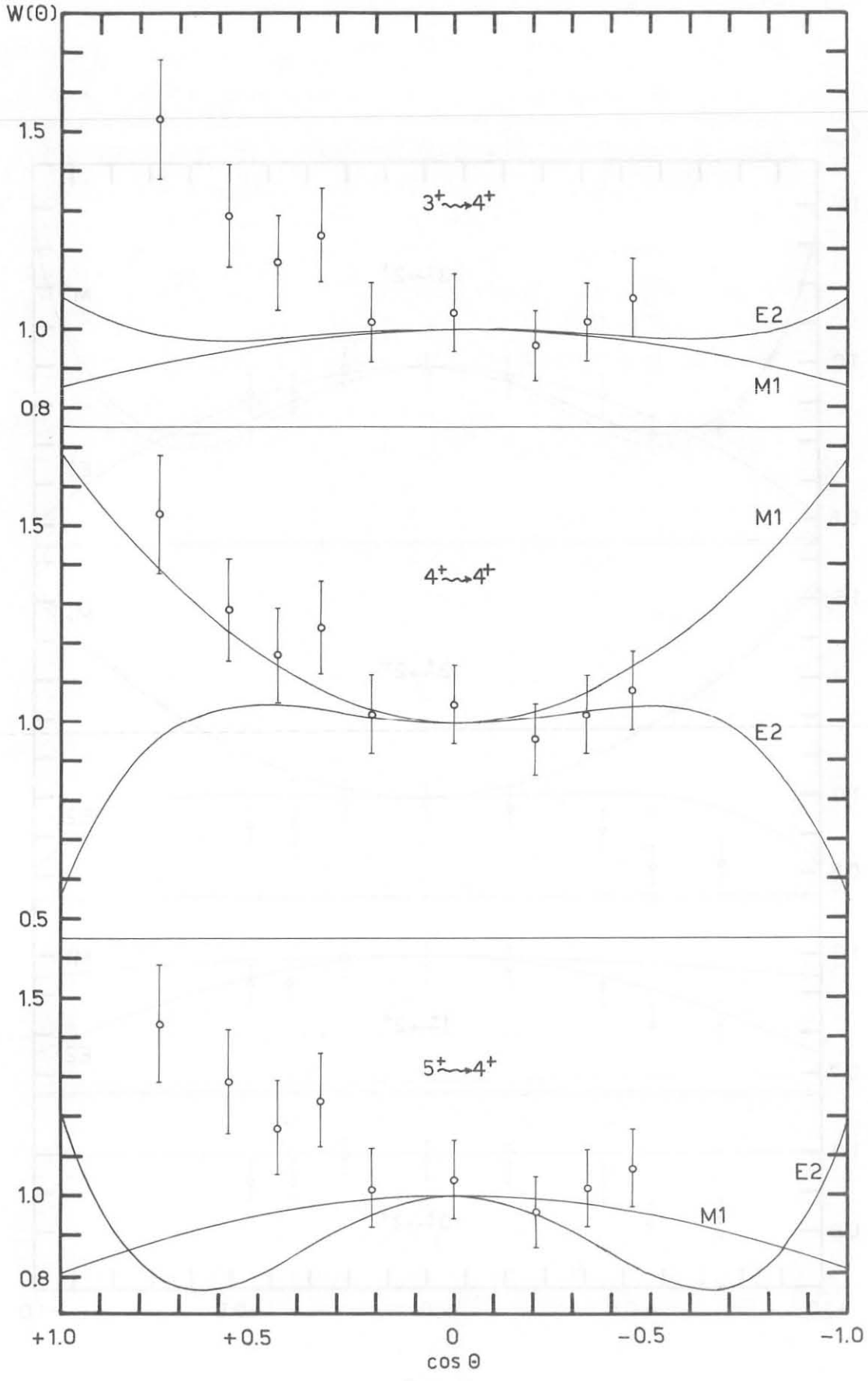
W(θ)
1.5
1.0
0.8
3+ → 4+
E2
M1
1.5
1.0
0.5
4+ → 4+
M1
E2
1.5
1.0
0.8
5+ → 4+
E2
M1
+1.0
+0.5
0
−0.5
−1.0
cos θ

Fig. 10

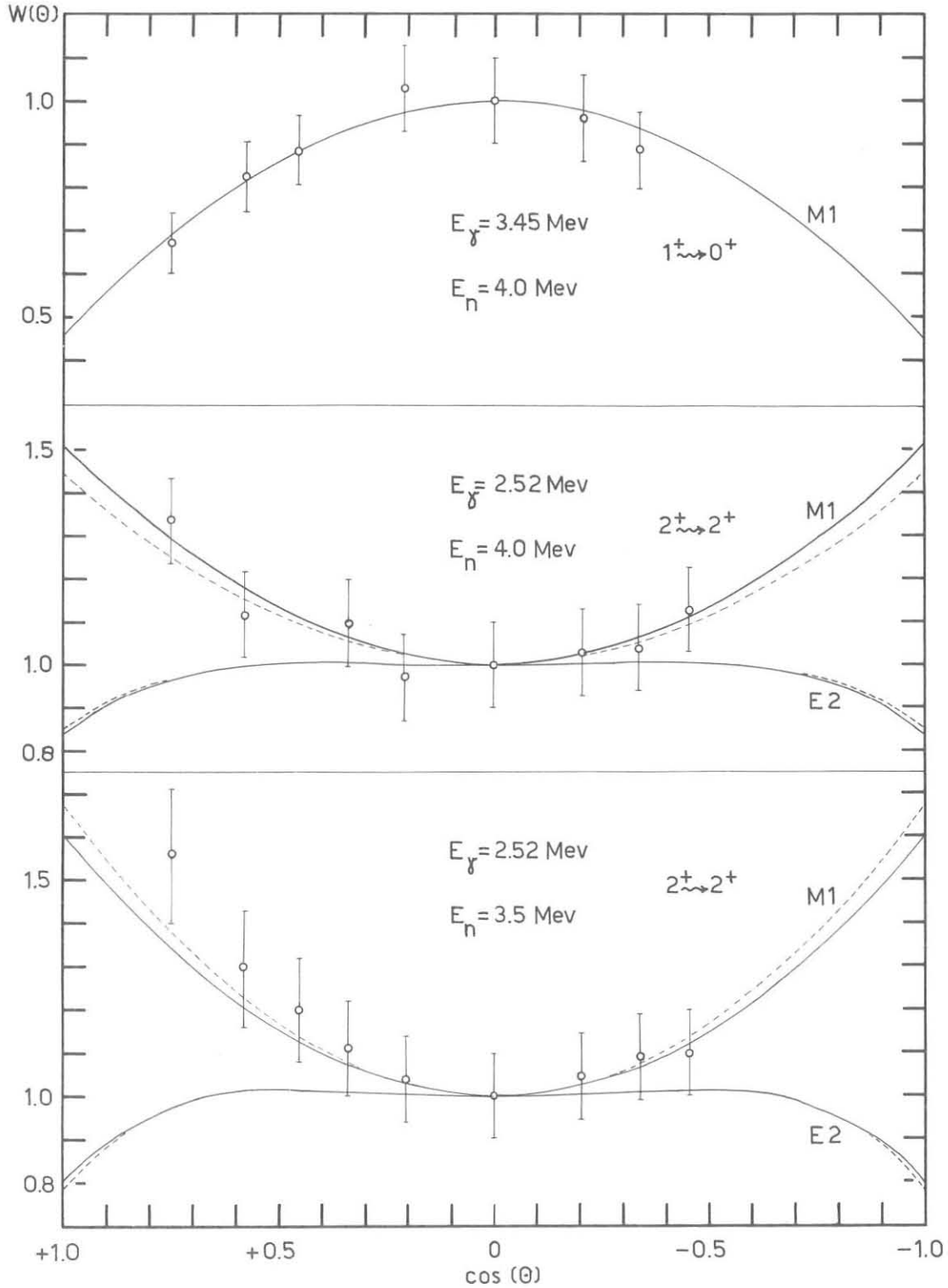
W(Θ)
1.0
0.5
E_γ = 3.45 Mev
E_n = 4.0 Mev
1+ ⇝ 0+
M1
1.5
1.0
0.8
E_γ = 2.52 Mev
E_n = 4.0 Mev
2+ ⇝ 2+
M1
E2
1.5
1.0
0.8
E_γ = 2.52 Mev
E_n = 3.5 Mev
2+ ⇝ 2+
M1
E2
+1.0
+0.5
0
−0.5
−1.0
cos (Θ)

Fig. 11